Journal of Materials Chemistry A

Accepted Manuscript

ROYAL SOCIETY OF CHEMISTRY

www.rsc.org/materialsA

Journal of Materials Chemistry A RSCPublishing

ARTICLE

Multiple doping of graphene oxide foams and quantum dots: new switchable systems for oxygen reduction and water remediation

Cite this: DOI: 10.1039/x0xx00000x

Received 00th January 2012,
Accepted 00th January 2012

DOI: 10.1039/x0xx00000x

www.rsc.org/

M. Favaro,[a,b] F. Carraro,[a] M. Cattelan,[a] L. Colazzo,[a] C. Durante,[a] M. Sambi,[a] A. Gennaro,[a] S. Agnoli,[a]* and G. Granozzi[a]

Single- and multi- Boron, Nitrogen, Sulphur doped graphene oxide quantum dots and three-dimensional foams are synthesized by a simple and environmental friendly electrochemical method. The electrochemical activity of these materials in the oxygen reduction reaction is investigated by cyclic voltammetry and rotating disk electrode measurements. The experimental data demonstrate that the reaction selectivity is controlled by the oxidation degree of the materials: as-prepared graphene oxide quantum dots, which present highly oxidized functional groups, follow a two-electron reduction pathway and produce hydrogen peroxide, whereas after a reduction treatment by $NaBH_4$, the same materials favour a four-electron reduction of oxygen to water. The high selectivity and high efficiency of the graphene oxide quantum dots for the production of hydrogen peroxide can be efficiently used for water remediation applications (phenol decomposition).

Introduction

From the large ensemble of graphene related materials, Graphene Oxide (GO) has clearly emerged as the most versatile building block for the development of complex three-dimensional (3D) architectures and functional nanosystems. The undisputed success of GO in several areas of science and technology is due to its remarkable physicochemical properties associated with low cost, easy processing and large yield production. After ten years of intense research, this material still represents the most important wet chemistry-derived precursor for graphene synthesis, to which it can be easily converted either by chemical or thermal reduction processes, and it is the acknowledged workhorse for most technological applications.[1,2,3]

GO consists of a single-layer of graphite oxide and is usually produced by the oxidation of graphite and subsequent dispersion and exfoliation in water or suitable organic solvents.[1] By means of different approaches, such as vacuum filtration,[3,4] freeze-pump-thaw,[3] and spin-coating,[4] GO can be used for the preparation of high surface area graphene-based 3D structures and can also be easily functionalized to obtain Chemically Modified Graphenes (CMGs).[5] These materials have drawn a tremendous interest in the literature, thanks to their remarkable catalytic activity for several different chemical reactions.[3,4,6,7,8] The new reactivity stems from the introduction of heteroatoms or specific functional groups in the honeycomb lattice, which afford a fine control of new chemical properties with high specificity.[9,10] Several heteroatoms have been successfully introduced in the carbon lattice, such as nitrogen, boron, sulphur, phosphorus and, more recently, combinations of these elements in order to achieve selective dual doping.[6,9,10,11,12,13,14,15,16,1718] These CGMs have shown quite interesting properties in terms of electroactivity, in particular in the case of the oxygen reduction reaction (ORR).[6,9,14,19,20,21,22]

Very recently, another rising star among graphene related materials is represented by Graphene Quantum Dots (GQDs), that are graphene materials characterized by few layers and lateral dimensions of few nanometers.[23,24,25] Since graphene exhibits an infinite exciton Bohr radius, quantum confinement can take place in graphene systems of any finite size, paving the way to several interesting phenomena that cannot be obtained in other semiconductors.[23,26] The energy band gap between the HOMO and LUMO of a sp^2 carbon honeycomb lattice can be varied from 0 eV,[27] in the case of a flat and micrometric sized monolayer graphene, to 4.4 eV in benzene,[28] simply by varying the size of the GQD.[23,26,27] Consequently, GQDs, as a new kind of quantum dots, have emerged in the last few years and have kindled a large research interest. Due to the pronounced quantum confinement and edge effects, GQDs can assume novel chemical/physical properties that are promising for different

applications in the fields of optolectronics, photocatalysis, sensing and bio-recognition.[29,30,31] Several efforts have been focused on the development of synthetic protocols for the preparation of GQDs, either by top-down or bottom-up methods. In a recent paper, we have shown how to prepare GO quantum dots (GOQDs) solutions by means of a simple electrochemical (EC) procedure starting from GO electrodes.[32,33] Following this approach we have prepared single-(B and N) and multi-doped (N,B) GOQDs.[34] We have studied the catalytic activity toward the ORR of these doped GOQDs, observing a clear improvement of the efficiencies in presence of the single dopants, which is further boosted when both B and N are present. Notably, we have found that the selectivity toward ORR in GOQDs can be easily switched from a two electron path to a four electron path by simply controlling the oxidation degree of the materials. In this work, taking the cue from these results, we have further extended the series to S- and S,N-doped GOQDs. We report here a complete structural study for the whole series by X-ray Photoemission Spectroscopy (XPS), Near Edge X-ray Absorption Fine Structure spectroscopy (NEXAFS), Raman spectroscopy and scanning tunnelling microscopy (STM). Their photoluminescence (PL) properties have been also determined. We demonstrate that the S and S,N-doped GOQDs show a very high catalytic activity toward ORR, in line with our previous data with other dopants.[34] In addition, we report here that doped-GO foams can be obtained during the synthesis of doped-GOQDs.[32] These materials, which associate the benefits of the chemical doping with a high surface area, can be used as efficient electrodes for the cathodic compartment of fuel cells.

Finally, thanks to the high selectivity toward the production of hydrogen peroxide exhibited by the as-prepared doped-GOQDs, we demonstrate that the latter can be suitably employed for water remediation thanks to the hydrogen peroxide oxidative property.

Results and discussion

A GO electrode was electrochemically etched during anodic and cathodic CV between -3.0 V and +3.0 V (vs. $Ag/AgCl/Cl^-_{(sat.)}$), up to thousands cycles, in a PBS.[32,33] For the synthesis of doped-GOQDs (as described in detail in our previous work),[34] a dopant molecule such as 1,4-phenylenebis(boronic acid), ethylendiamine, 1,10-phenantroline or α-lipoic acid was added into the electrolytic solution to provide the dopant heteroatoms. Similarly, to prepare co-doped-systems as B,N- or S,N-GOQDs a mixture of dopant molecules (or L-cysteine, in case of S,N-co-doping) was added to the electrochemical solution.

A. Chemical and structural characterization

XPS measurements were performed to determine the chemical composition of the doped-GOQDs. The C/O atomic ratio, equal to 4.3, is almost alike for all doped GOQDs, with only slight differences. Table 1 reports the C/dopant stoichiometry for all the prepared systems calculated from the XPS data, which are similar in terms of dopant concentration to those already reported in the literature for analogous materials.[24,25,29,30]

To determine the chemical state of dopants atoms, high-resolution XPS peaks of carbon and doping elements were separated into single chemically-shifted components. For the B- N- and B,N-GOQDs the data have been already reported in ref. 34, and they will be not discussed further here. The S-doped GOQDs (hereafter S-GOQDs) show the presence of the –CS component in the C 1s photoemission spectrum, reported in Figure 1.a, centred at 285.5 eV.[25,35] In the multipeak analysis of the S 2p photoemission line (reported in Figure 1.b, bottom) the main component (2, 164.1 eV), which represents the 85% of the whole S 2p peak, is constituted by –C–S–C– thiophenic like units.[25,35] A weak component, associated with –SH,[25] is also present at 162.5 eV (1). Finally, two weak components (contributing to the S 2p photoemission line for the 4% of the total integrated area) are localized in the high BE tail at, 168.2 eV (3) and at 169.3 eV (4), and correspond to $–C–SO_2–C–$ and $–C–SO_3–C–$ groups, respectively.

Table 1. C/dopant stoichiometry (calculated from XPS quantitative analysis) for the doped-systems studied in this work.

	B ($\%_a$)	N ($\%_a$)	S ($\%_a$)
B-GOQDs	5.3	-	-
N-GOQDs	-	5.1	-
S-GOQDs	-	-	4.9
B,N-GOQDs	5.2	4.7	-
S,N-GOQDs	-	4.8	5.4

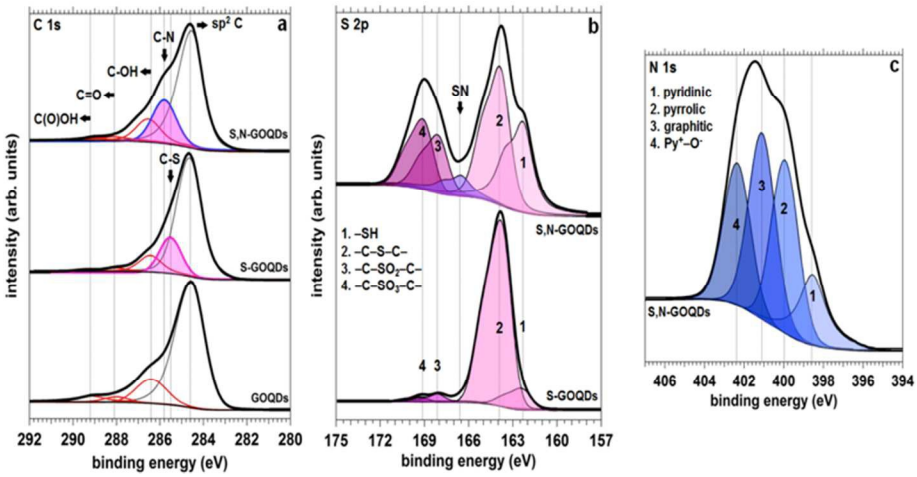

Fig. 1. a: Multicomponent analysis of the C 1s XPS peaks for pure, S- and S,N-GOQDs. Figures b and c report the relative dopant photoemission line fits, for S 2p and N 1s photoemission lines, respectively.

As reported before,[34] the synthesis mechanism provided by the electrochemical etching of a GO WE in presence of a molecular dopant affords the introduction of in-plane doping, and edge functionalization, with the consequent formation of very active catalytic sites for ORR. [9,10,14,34-35] Since synergetic effects between different heteroatoms present in the graphitic networks lead to higher catalytic reactivity toward several electrochemical reactions (and, in particular, ORR),[6,9,12,34-36,37,38,39] we employed a simple amino acid, such as L-cysteine, for preparing S,N-co-doped GOQDs (hereafter S,N-GOQDs).

Regarding the S,N-GOQDs, the C 1s fit reported in Figure 1.a, shows the presence of both –CN and –CS components.[12,38,39,40] Since they are found in the same spectral region, it is not possible to single out the individual contributions; therefore only one intense peak (centered at 285.7 eV) can be identified. The fit of the S 2p photoemission line (Figure 1.b, carried out with 2p doublets with fixed spin orbit splitting, set to 1.2 eV) confirms the presence of several different structural environments for sulfur. Five chemically shifted components can be identified at 162.3 eV, 163.9 eV, 166.5 eV, 168.1 eV and 169.1 eV, which are assigned to –SH groups (1, 28 %), thiophene-like groups (2, 40 %), -SN groups (8 %), -C-SO_2-C (3, 11 %) and –SO_3 (4, 13 %) groups, respectively.[25,35-40] Notably, it is possible to observe the presence of –SN groups that indicate the S,N co-doping of the GOQDs. Interestingly, the N 1s photoemission peak presents a multicomponent structure comprising pyridinic (1), pyrrolic (2), graphitic nitrogen (3), and pyridine N-oxide (4) groups, respectively (Figure 1.c), which is qualitatively similar to our previous results on N-GOQDs and B,N-GOQDs.[34] The presence of the –SN counterpart in the N 1s spectrum however, is not easy to detect, since the electronegativity of sulphur and carbon are very similar (in the Pauling scale, C= 2.55, S = 2.58 while N = 3.04). Therefore, such component will be superimposed to the signal of graphitic N-based groups (3) (i. e. in the range of 401.1-401.4 eV). This overlap is in good agreement with the higher intensity observed for this component in the case of S,N-GOQDs, in comparison to what is observed in the N-GOQDs (in fact, relatively to the total intensity of the N 1s spectrum, the content of this high BE component increases from 24 %, in the case of N-GOQDs, to 33 % for the S,N-GOQDs). Differently from B,N-GOQDs, sulphur seems to suppress the pyridinic group (N1, 398.6 eV) content in the N 1s spectrum, with a decrease from 25 % to 17 % passing from N- to S,N-GOQDs. Similarly, the same trend is observed for the pyrrolic group (N2, 399.9) amount (from 41 % in the case of N-GOQDs to 28 % in the case of S,N-GOQDs). Finally, relatively to the total intensity of the N 1s spectrum, the content of the higher BE component (N4, assigned to pyridine oxide groups centred at 402.4 eV) increases from 10 %, in the case of N-GOQDs, to 22 % for the S,N-GOQDs. The S,N-GOQDs show a higher amount of oxidized groups (both on N 1s and S 2p photoemission lines) than the N- or S-GOQDs. This can be rationalized by taking into account the C/O ratio that characterizes the dopant molecules. In fact, it is lower for L-cysteine (1.5) than for α-lipoic acid, which is also a strong antioxidant (4); furthermore, no C/O ratio can be defined for ethylendiammine or 1,10-phenantroline.

To gain a better understanding of the chemical nature of the doped and co-doped GOQDs, we carried out Near Edge X-ray Absorption Fine Structure (NEXAFS) measurements, as reported in Figure 2. For all the studied systems, the C K edge spectra show the presence of the main 1s-π* transitions typical of a partially oxidized graphene-derived material.[41] In particular, it is possible to observe the presence of the C=C (284.3 eV, π_1), C-OH (286.8, π_2), C=O (287.7, π_3) and COOH (289.1, π_4) transitions.[41,42,43] For the B- and the B,N-GOQDs, a new component, labelled as 1, is present in C K-edge spectra, centred at 282.7 eV. This component can be assigned to the presence of substitutional boron atoms. Moreover, in the case of N-, S-, B,N- and S,N-GOQDs, a

slight broadening of the π_1 peak, due to the presence of an additional component centred at about 285.3 eV is visible. This component, labelled as 2, is associated with the C–N or C–S bonds,[44] confirming the interpretation of photoemission data.

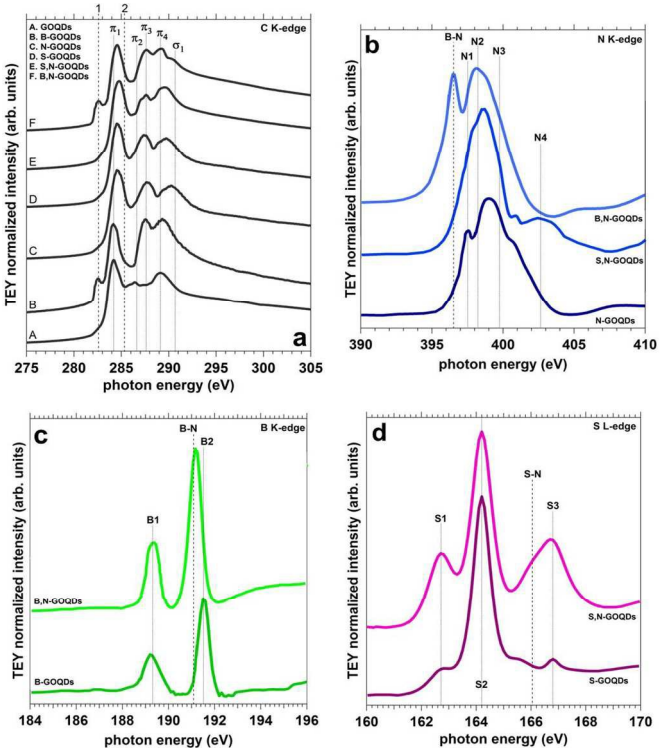

Fig. 2. NEXAFS spectra acquired in total electron yield (TEY) mode of the carbon (a), nitrogen (b), boron (c) K-edges and sulfur L-edge (d).

As it can be observed from Table 2, (which reports the values of the BEs for the single chemical components derived from the fits of the XPS data and the photon energy of the relative resonances observed in the NEXAFS spectra), the detailed analysis of the absorption edges of the dopant elements basically confirm the results obtained from the XPS measurements. In the case of N- and S,N-GOQDs, the N K edge spectra show the 1s-π* transitions due to the pyridinic (N1, 397.5 eV), pyrrolic (N2, 398.3 eV) and graphitic (N3, 399.8 eV) species.[45] The peak centred at a photon energy of 402.7 eV (N4) is related to the 1s-σ* transition of the N–O groups. Regarding the B,N-GOQDs a further peak can be observed for a photon energy of 396.6 eV, which is connected to the B-N bonds. In the case of S- and S,N-GOQDs, the S L edge spectra show the presence of –SH (S1, 162.8 eV), C–S–C (S2, 164.2 eV) and $–SO_3$ (S3, 166.8 eV) groups. In particular, for the S,N-GOQDs, a broad peak is observed for a photon energy between 165 and 168 eV, due to the concomitant presence of a relatively high amount of oxidized S-based groups and S-N groups, whose 1s-π* transition is centred at 166.1 eV. Similarly, the B K edge spectrum of B-GOQDs is characterized by the presence of two distinct peaks, associated with the 1s-π* (at 189.3 eV) and 1s-σ* (at 191.5 eV) absorption transitions of the B–sp^2 C and C-BO_2 groups, respectively. In the case of B,N-GOQDs, a further feature can be observed at 191.1 eV, due to the presence of C–BNO bonds, wherein the boron atom is bonded to a nitrogen and an oxygen atom.

Raman microscopy was carried out to confirm the graphenic structure of the materials and to study the local loss of symmetry in the doped-GOQDs due to the introduction of heteroatoms in the graphene-like structure. Figure 3.a compares the Raman spectra for the different systems. Three bands are clearly observable,[46] the G band, at about 1600 cm^{-1}, the D band 1350 cm^{-1} and, at 1620 cm^{-1}, the D' band that, for highly defective materials, is usually detectable as a shoulder of the G band.[46,47] The D and D' modes are observed only in the presence of defects that lead to the breaking of the D_{6h} symmetry of the graphitic honeycomb lattice (such as dopant atoms).[47] In the literature, Raman studies where the size of pure GOQDs is related to their G band full width at half maximum (FWHM), G band position and D/G intensity ratio have been widely reported.[48] In our case, the presence of the D' band is clearly visible as a shoulder in the G band in most spectra, which is the reason why it is quite difficult to determine precisely the G band position and FWHM.

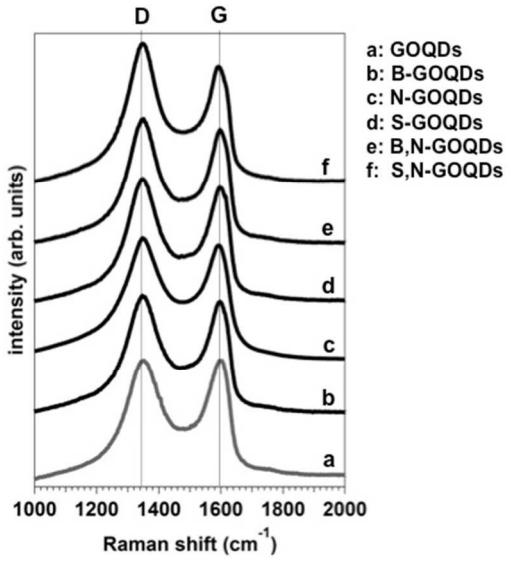

Fig. 3. Raman spectra of pure and doped-GOQDs in the D-G band region.

This analysis is even more complicated if one considers that changes in these two parameters can be related to electronic doping, which can be induced by the presence of heteroatoms in the system.[49,50] In the spectra in Figure 3.a the only spectral difference between the samples is represented by the noticeable shift of the G band position of pure GOQDs centred at about 1600 cm^{-1}, with respect to the other preparations, which range from 1592 to 1596 cm^{-1}. This can be related to a larger crystalline size due to the absence of dopants.[48]

Journal of Materials Chemistry A RSCPublishing

ARTICLE

Table 2. Spectral data of the studied systems. All the values are in eV, and the ones reported between parentheses are the energies of the resonances observed in the NEXAFS spectra.

C 1s (K-edge)		N 1s (K-edge)		S 2p (L-edge)		B 1s (K-edge)	
C=C (π_1)	284.6 (284.3)	Pyridinic (N1)	398.6 (397.5)	-SH (S1)	162.3 (162.8)	B-sp^2C (B1)	189.6 (189.3)
C-OH (π_2)	286.4 (286.8)	Pyrrolic (N2)	400.0 (398.3)	C-S-C (S2)	163.9 (164.2)	C-BO/C-BN	190.6
C=O (π_3)	288.1 (287.7)	Graphitic (N3)	401.1 (399.8)	C-SO_2-C	168.1	C-BNO	191.1 (191.1)
COOH (π_4)	289.2 (289.1)	N-O (N4)	402.4 (402.7)	-SO_3 (S3)	169.1 (166.8)	C-BO_2 (B2)	191.5 (191.5)
B-sp^2C (1)	283.5 (282.7)	B-N	397.5 (396.6)	S-N	166.5 (166.1)		
C-N (2)	285.8 (~285.3)						
C-S (2)	285.5 (~285.3)						

In order to determine the morphological properties of the GOQDs we have carried out STM measurements. High-resolution topographies indicate that the pure GOQDs exhibit a quasi-circular shape (Figure 4.a), whereas B-, N-and S-GOQDs (Figure 4.b,c,d) show mainly straight edges resembling triangular shapes. As regards the co-doped systems, straight and round mixed edges are observable on the B,N-GOQDs (Figure 4.d), whereas the S,N-GOQDs are mostly characterized by a round shape. Figure 4.g reports a small area image on single GOQD for the prepared systems, where the morphology differences described above are better emphasized. The average size of the observed pure, doped and co-doped-GOQDs is about 2 nm, with rather sharp size dispersion (σ=1 nm). The average height is in the 0.4-0.6 nm range, confirming that the prepared GOQDs are constituted by a single-layer of pure or doped GO.

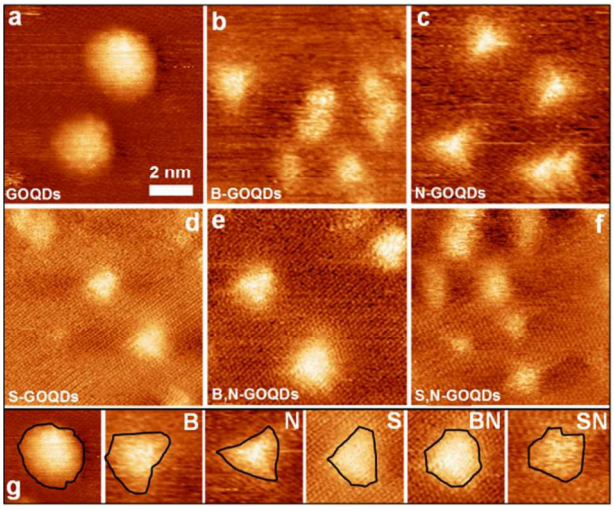

Fig. 4. STM topographies (10 × 10 nm) of pure (a) and doped (b–d) GOQDs at the HOPG/air interface; a: GOQDs; b: B-GOQDs; c: N-GOQDs; d: S-GOQDs; e: B,N-GOQDs; f: S,N-GOQDs; g: single GOQD for the different systems: the black line emphasizes the distinct edge morphologies (Figures a, b, c and e are adapted and reprinted with permission from ref. 34, Copyright 2015 American Chemical Society).

No atomic resolution of the carbon lattice is observed probably because of close proximity of edges and presence of defects that scatter the electron wavefunctions.[51,52]

B. Photo-physical properties of pure and doped-GOQDs

The chemical doping of the GOQDs leads to interesting photo-physical properties, as reported in Figure 5. Since graphene and GO QDs have only recently emerged in the literature, the comprehension of the origin of their PL properties is still a matter of debates. One common feature of the PL of graphene-based QDs is the excitation dependence of the emission wavelength and intensity. However, whether this occurs because of the optical selection of differently sized nano-platelets (quantum confinement effect, QCE) and/or different emissive traps on the QDs surface,[53] is currently unresolved and not yet well-understood.[23,24,30] Moreover, it has been largely demonstrated[23,30] that the synthesis protocol used to produce graphene-based QDs can substantially modify their photo-physical properties, probably due to different oxidation states ("surface passivation") of the nano-sized graphene platelets. Thence, the combination of incomplete understanding of the PL mechanisms with the sensitive dependence on the synthesis conditions of the photo-physical properties makes a direct comparison with literature data obtained on other materials difficult.

Regarding the UV-Visible absorption spectra of the prepared systems (black spectra in Figure 5), it is important to highlight that the π-π* first order transition band for the doped-GOQDs is red-shifted with respect to pure GOQDs (centred at 252 nm, Figure 5.a) in all the investigated cases (and in agreement with what has been observed in previous works[23,24,30]). In fact, the B-GOQDs are characterized by an absorption band centred at 282 nm (Figure 5.b), with a less intense shoulder at 308 nm, whereas the N-GOQDs (Figure 5.c) exhibit an intense absorption band at 280 nm, with a shoulder centred at 312 nm. The S-GOQDs (Figure 5.d) are instead characterized by an absorption band centred at 340 nm, whereas the B,N- and S,N-GOQDs (Figure 5e,f) show absorption features at 285 nm and 338 nm, respectively. The introduction of dopants can therefore promote a more intense light adsorption in the visible

range, which can be exploited for more efficient energy conversion in different types of nanosystems.

Switching to PL data, the undoped GOQDs (Figure 5.a) show a quite complex emission spectrum where different components can be observed. Albeit the spectra are strongly dependent on the excitation and on the type of materials, two main broad emission bands can be observed: a violet-blue emission around 420-450 nm and a broad "green" emission, centred around 480-520 nm, as already reported in other studies[23,24,30,54]. The "blue" emission can be associated with the band to band π*-π transitions connected to the existence of domains of sp^2 carbon atoms, whose energy is strongly size-dependent.[55]

The structural properties of GOQDs strongly affect the optical properties: "blue luminescence" is more intense in the case of N- (Figure 5.c), S- (Figure 5.d) and S,N-GOQDs (Figure 5.f), where the emission (acquired under irradiation at 340 nm) is blue-shifted to 410 nm, 430 nm and 415 nm, respectively, with respect to pure GOQDs (450 nm). In the case of N-GOQDs, this observation is in agreement with the literature.[56,57] In fact, it has been reported that the relatively high electron withdrawing ability of N atoms within the conjugated C plane generates a distortion in the HOMO (π)-LUMO (π*) structure of the graphitic core of the GOQDs, leading to a band gap consistent with blue emission as a result of an intraband exciton annihilation (a π-π* electron-hole recombination).[58,59] Moreover, N-GOQDs show a well-defined and narrower emission band than pure counterparts. The PL spectra of N-GOQDs exhibit a double peak structure, whose components are centred at 388 nm and at 420 nm, respectively. The detailed origin of this doublet under UV irradiation is not yet well understood.

In the case of B,N-GOQDs the PL spectrum acquired at 340 nm is constituted by two peaks, centred at 400 nm and 440 nm, respectively. Differently from what is commonly observed for graphene and GO-QDs, the increase in the excitation wavelength determines a strong increase in the intensity of the PL emission, in particular for excitation wavelength beyond 450 nm. According to our knowledge, this behaviour has not been reported in other studies so far, and it is still under our investigation.

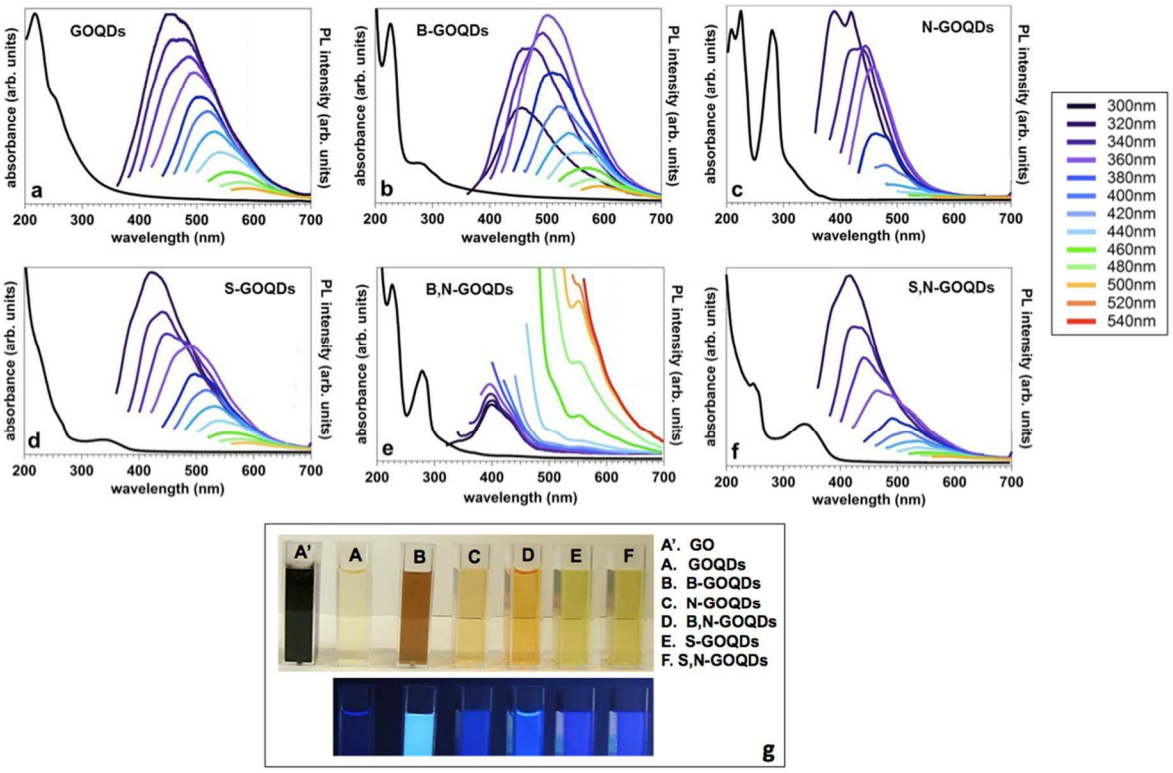

Figure 5. UV-Visible absorption and PL spectra acquired at different excitation wavelengths for pure (a), B- (b), N- (c), S- (d), B,N- (e) and S,N-GOQDs (f). Figure g reports the digital image of the prepared systems under environmental and UV light (254 nm).

The PL properties in the green range exhibit a very complex behaviour, especially in the case of dually doped systems, where the presence of different emission channels can be easily observed. Most recent works suggest that "green" PL is connected to the interstate to band n-π transitions triggered by oxygen[60] and dopant-related[61] defects. This type of emission is just weakly dependent on the dimensions of the QDs, whereas it is controlled by the position of the defect states and therefore by the type of dopants and of

edge functionalization. The PL emission originated by these processes is just weakly dependent on the exciting radiation (see for example the clear emission line at 560 nm in B,N-GOQDs), nevertheless the possible interaction between different decaying channels makes the PL spectrum quite complex as a function of the exciting radiation.

Concerning the S,N-GOQDs, to our knowledge the only studies present in the literature on the S,N co-doping of graphene-based nano-platelets are the works of Zhang et al.,[62] Dong et al.[63] and Qu et al.;[64] in the latter, in particular, the authors obtained S,N-graphene QDs (GQDs) via hydrothermal synthesis using thiourea as the S,N molecular source. They reported a PL spectrum (under irradiation at 340 nm) centered at about 450 nm, which was scarcely dependent on the energy of the exciting radiation. According to the authors, in this case PL emission is mainly due to the π^*-π transitions from the graphitic sp^2 core, whose electronic levels are slightly perturbed by the presence of dopants. Figure 5.g reports the digital images of the prepared systems, under environmental and UV light. As it is possible to observe, all the studied systems are characterized by strongly dopant-dependent optical properties.

Finally, we want to stress the fact that the differences in the optical properties observed for the distinct systems are influenced only by the different chemical doping, and not by size effects, as it can be deduced by the results of the STM investigation (Figure 5.)

C. Oxygen reduction catalytic activity of pure and doped-GOQDs.

Figure 6 reports the CV polarization curves taken at different scan rates in a 0.1 M KOH solution saturated with O_2, for pure (a), S- (b) and S,N-GOQDs (c). At variance with the other dopants, sulfur has an electronegativity very similar to carbon (S: 2.58, C: 2.55), but with a larger atomic radius (the atomic radius passes from 67 pm for C to 88 pm for S)[65]. Therefore the incorporation of S into the sp^2 carbon lattice can induce strain that may change the charge distribution and facilitate oxygen chemisorption, without injecting or withdrawing charge as result of an electronegativity-induced polarization effect.[18] Alternatively, other authors suggest that the most critical parameter for explaining the chemical activity in the ORR is the spin density modification induced by the dopant or by dopant-related defects.[66,67]

Theoretical investigations of the ORR activity of thiophenic S indicate that the active sites are the first or second neighbour carbon atoms;[68] some authors however point also to the activity of sulfonic groups (-SO_2-) and suggested that these are responsible for the most energetically convenient reaction path for the four-electron reduction of oxygen to water.[67]

The values reported in Table 3 indicate a drastic increase in the catalytic activity of the material doped by S, as expected on the basis of the structural data provided by XPS, indicating a large fraction of thiophenic groups. In particular, the onset of the ORR is, for the S-GOQDs, shifted by 113 mV with respect to pure GOQDs. The S,N-GOQDs also show a high catalytic activity toward ORR. As shown by Table 3, the synergistic effect of the co-doping influences the reduction potential onset, which is 21 mV more positive than in S-GOQDs, with an overall gain of 134 mV with respect to the pure GOQDs. This is in line with the previous results obtained on other doped-GOQDs.[34] To conclude, the graphitic basal plane is characterized by a poor catalytic reactivity (as demonstrated by the highly negative O_2 reduction potential of pure GOQDs);[69] thus, the introduction of different heteroatoms, irrespectively of the particular mechanism that activates the oxygen adsorption, dramatically increases the activity, with the consequent decrease of the overpotential for the reduction of oxygen on doped-GOQDs.

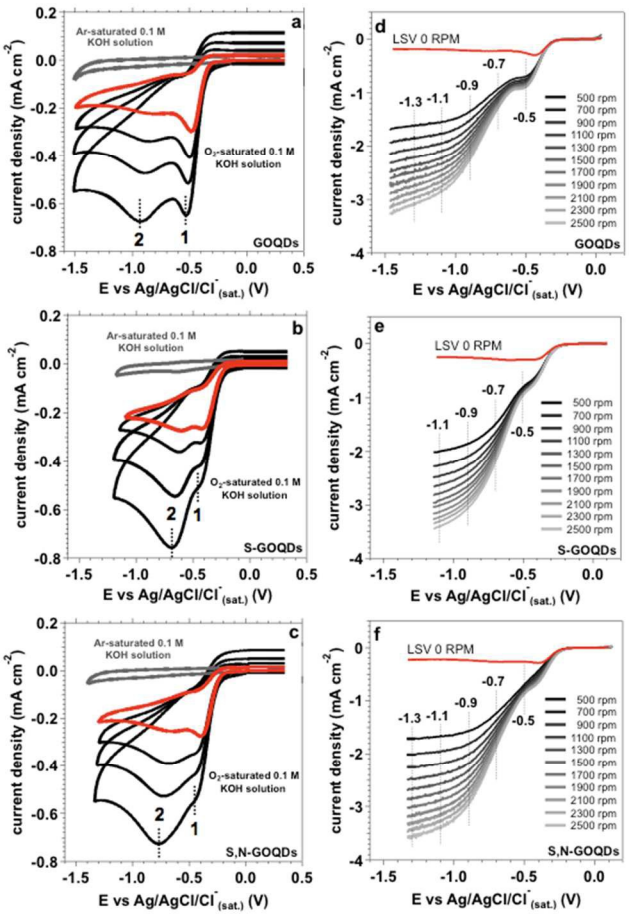

Fig. 6. CVs of pure- (a), S- (b) and S,N-GOQDs (c) in O_2-saturated 0.1 M KOH solution, at different potential scan rates (10, 20, 50 and 100 mV/s). For each system, the grey polarization curves (at 10 mV/s) are recorded in Ar-saturated 0.1 M KOH solutions; d, e, f: RDE linear sweeps for pure-, S- and S,N-GOQDs, respectively, acquired in O_2-saturated 0.1 M KOH solution for different rotation speeds.

Tafel plots obtained by RDE measurements are reported in figure S1 (see ESI), however the presence of several types of catalytic sites with similar activity prevents a clear identification of reaction mechanism.

Nevertheless, as a general trend, it can be seen that in the case of doped systems, higher current densities can be obtained by applying lower potentials (or, analogously, in the case of the doped-GOQDs for a fixed potential it is possible to obtain higher current densities with respect to pure GOQDs). This phenomenology is enhanced passing from the single to the dual-doped GOQDs

Moreover, as well documented by Figure 6, two distinct features (labelled as 1 and 2) are observed in the voltammetric responses of the pure and S-GOQDs. Figure S2 (see ESI) reports the peak current densities for peaks 1 and 2 for pure (a), S- (b) and S,N-GOQDs (c) as a function of the square root of the scan rate.

In all the cases, the trend is linear, meaning that both the observed voltammetric features (1 and 2) are diffusion peaks more likely connected to the irreversible reduction of oxygen on different catalytic sites that are sequentially activated by the increase of the scan rate,[70,71] and that are probably located on the edges and on the basal plane of the GOQDs, respectively.[54,71,72] This is in line with previous works in the literature, which state that in graphene the edges are characterized by higher electroactivity than the basal plane because of the distortion of the electronic density and of the possible presence of special functional groups.[72]

On the S-GOQDs the sulphur dopant is exclusively localized on the edges in a thiophenic configuration (see XPS analysis), therefore the edge sites should exhibit a clear different electrochemical activity with respect to basal plane sites. On the other hand, on the S,N-GOQDs, the peak 1 connected to the reduction of oxygen on the edge sites is present only as a minor shoulder of the main peak (2), generated by the basal plane sites. From the comparison between pure and S,N-GOQDs, it results that the peak 2 is characterized by a shift of about 170 mV toward less cathodic potentials, due to the presence of the N substitutional defects that boost the activity of the basal plane. Therefore, the difference of the electroactivity between edge and basal plane sites is rather small. Figure S3 reported in the ESI, shows a graphical schematization of the reduction mechanism of oxygen on the different active sites. Finally, the co-presence of N and S in the same graphenic structure leads to a clear synergistic effect on the oxygen electroreduction. By comparing the overpotentials of peak 1 of the S- vs S,N-GOQDs, it is possible to see that the dually doped materials show a net gain in the overpotential of about 20-30 mV with respect to the S-GOQDs. The best performance of multi doped materials is also in agreement with previous results on the B,N-GOQD system[34].

In order to determine the number of the exchanged electrons during the irreversible reduction of oxygen and, in this way, to clarify the reaction mechanism on the doped-GOQDs, we carried out rotating disk electrode (RDE) measurements. Linear Sweep Voltammetry (LSV) curves of the ORR on the studied systems are reported in Figure 6d, e and f. recorded for different electrode rotation at a scan rate of 10 mV/s (the corresponding Koutechy-Levich analyses are reported in Figure S4). For the calculation details, see the experimental part reported in ESI. Table 3 reports the number of the electrons exchanged during the irreversible reduction of oxygen, determined by the Koutechy-Levich linear fits reported in Figure S4.

All the as-prepared systems are characterized by a two electron ORR mechanism with the only exception of the S-GOQDs that show an O_2 reduction pathway close to a four electron mechanism. This result can be explained assuming that the S-doped system is characterized by a lower oxidation degree with respect to the other investigated materials and, in particular, to the S,N-GOQDs (as shown by the XPS measurements reported in Figure 1). As we have demonstrated in our previous work,[34] the presence of oxidized dopant groups on nanometric graphene patches has a negative effect on the catalytic activity and, in particular, on the four electron mechanism selectivity. This result seems also to substantiate a more general relationship recently proposed for multi-doped carbon materials, which establishes a correlation between work function and ORR activity: doped materials with low work function values exhibit the best performances in ORR and the best selectivity of the four-electron reduction path.[73]

Durability tests carried out on N- and N,S-GOQDs (See figure S5 in ESI) indicate that the materials show performances very similar if not better with respect to commercial Pt catalyst (20% Pt on Vulcan XC72). Notably, the electrocatalytic activity of doped GOQDsis not affected by the presence of methanol in the reaction environment up to a concentration of 0.5 M. This high tolerance is common to other doped nanocarbon catalysts.[9]

Taking the cue from the results obtained for the S-GOQDs, we induced a four electron pathway in the S,N-GOQD system by performing a mild chemical reduction with $NaBH_4$ for 12 h at r.t., as already performed in an our previous study[34] (for the details, see the experimental part reported in ESI). Figure 7 a**,** b and c reports the S 2p and the C and N 1s photoemission lines de-convoluted into chemically shifted components, for the S,N-GOQDs after the chemical reduction (hereafter, red-S,N-GOQDs). In this case, in addition to the important decrease in the oxygen functional groups, it is possible to observe that the amount of C-S-C component increases considerably (from 40 % in the case of S,N-GOQDs to 62 % after reduction, relatively to the total S 2p area). This has a twofold effect: the oxygen reduction potential onset moves to -0.158 V, with a positive shift of almost 20 mV with respect to the onset of S,N-GOQDs and the reaction shows a strong selectivity toward the four electron reduction path. In fact, the Koutecky-Levich linear fits, reported in Figure 7.f and derived from the RDE measurements reported in Figure 7.e, show that the

n value is close to 4 and remains essentially constant over a potential window from -0.5 V and -1.1 V (see Table 3).

Moreover, it is important to stress the important increase in the concentration of the pyridinic groups after the chemical reduction treatment, triggered by the reduction-induced conversion of the pyridine oxide groups (present in relatively large amounts in the as-prepared S,N-GOQDs, see Figure 1.c). The pyridinic groups pass from 17 % in the case of S,N-GOQDs to 28 % for the red-S,N-GOQDs. As well documented in the literature, it is known that the pyridinic groups are highly active toward the four electron mediated reduction of oxygen,[25,74,75] especially in alkaline conditions.

Interestingly, from the same experiment where the synthesis of the doped-GOQDs is obtained, it is also possible to obtain doped GO porous films. As we have reported in our previous studies,[32,34] during the electrochemical synthesis of the GOQDs the •O and •OH species act as efficient scissors by reacting with the oxygen functional groups decorating the basal planes and the edges of the GO WE. These oxygen defects tend to line up and lead to an oxidative unzipping reaction,[76,77] resulting in the cutting of GO into smaller sheets.[24,32-34] This mechanism is similar to the Hummer's oxidation process of graphite, where epoxy groups are oxidized by •O, initially to epoxy and then to carbonyl pairs.[77] Moreover, during the electrochemical etching, the high potential values reached within the anodic and cathodic sweeps promote the intercalation/de-intercalation of ionic species present in solution, causing the expansion of the GO paper, the decoupling of GO sheets into single units and eventually the detachment from the electrode.

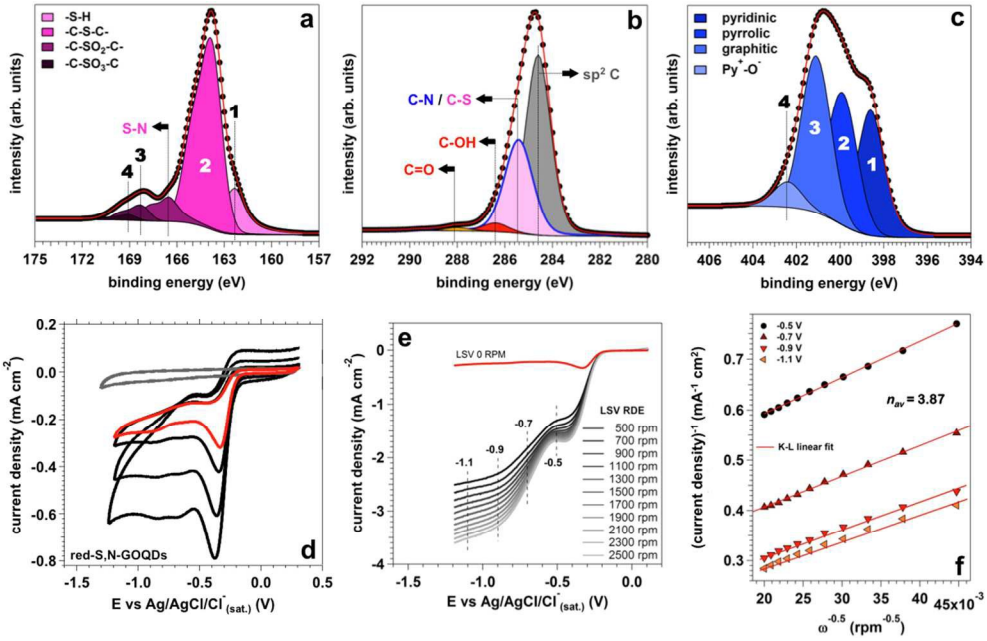

Fig. 7. XPS analysis and catalytic tests for red-S,N-GOQDs; a, b, c: multicomponent fits on S 2p, C and N 1s photoemission lines; d: CVs in O_2-saturated 0.1 M KOH solution, at different potential scan rates (10, 20, 50 and 100 mV/s). The inset reports the CVs (at 50 mV/s) acquired in Ar- and in O_2-saturated 0.1 M KOH solutions; e: RDE linear sweeps acquired in O_2-saturated 0.1 M KOH solution; f: Koutecky-Levich plots for different potentials derived from the RDE measurements. The average numbers of the exchanged electrons (n_{av}) reported in the figures have been obtained as average number of the values reported in **Table 3**.

Table 3. Potential onsets (derived by the tangent method), peak potentials (taken as the average between peak 1 and 2) and number of electrons exchanged

	Onset (V)[a]	E_p (V)[a]	n (E vs. Ag/AgCl/Cl$^-_{(sat)}$, V)[a]						
			-0.4	-0.5	-0.6	-0.7	-0.9	-1.1	-1.3
GOQDs	-0.311	-0.497	-	2.21	-	2.23	2.24	2.23	2.22
S-GOQDs	-0.198	-0.443	-	3.31	-	3.42	3.38	3.44	-
S,N-GOQDs	-0.177	-0.392	-	2.44	-	2.46	2.42	2.48	2.49
B-GOQDs [b]	-0.194	-0.456	-	2.31	-	2.35	2.28	2.26	2.30
N-GOQDs [b]	-0.198	-0.443	-	2.28	-	2.27	2.24	2.23	-
B,N-GOQDs [b]	-0.162	-0.374	-	2.50	-	2.49	2.48	2.62	-
red-S,N-GOQDs	-0.158	-0.334	-	3.87	-	3.86	3.88	3.88	-
red-B-GOQDs [b]	-0.169	-0.366	3.47	3.61	3.69	3.82	-	-	-
red-N-GOQDs [b]	-0.179	-0.354	2.86	3.36	3.42	3.78	-	-	-
red-B,N-GOQDs [b]	-0.143	-0.316	-	3.87	-	3.91	3.92	3.94	-

[a] The values are calculated for a potential scan rate of 10 mV/s.

[b] Onset, peak potentials and number of exchanged electrons are taken from ref. 34.

As a consequence of the electrochemical cycling, the pristine GO/GC electrode is deeply carved into a foam exhibiting a peculiar morphology (see Figure 8). The removal of small GOQDs produce a mesoscale porosity,[32,78] whereas overall the process of etching determines the formation of micrometric channels whose dimension and connectivity are strongly dependent on the pH.[32] Interestingly, selected heteroatoms can be introduced on the electrode surface as a consequence of the radical reactions at the basis of the etching process,[34] as demonstrated by XPS measurements (see ESI, Figure S6). For the attribution of the BEs of the single chemically shifted components, see above and ref. 34. The electrochemical etching therefore represents a quite versatile route for the preparation of multi doped 3D architectures based on GO through a simple one-pot synthesis that can be conveniently performed at r.t. and does not imply the usage of toxic or hazardous reactants such as NH_3 o H_2S.[11,13,14] Notably, by choosing the proper combination of dopant sources, the insertion of multiple combination of heteroatoms can be easily obtained. Here we report the catalytic tests performed on the co-doped GO foams, since the corresponding GOQDs are characterized by the highest activity among all the other prepared systems. The surface morphology of pure, B,N- and S,N-co-doped GO foams (hereafter GO, B,N- and S,N-GO foams, respectively) are reported in Figure 8, and show a quite complex morphology. Figure 9 reports the voltammetric responses for the O_2 reduction on pure- (a-d), B,N- (e-h) and S,N-GO foams (i-n) acquired in O_2-saturated KOH 0.1 M solution.

Table 4. Potential onsets (derived by the tangent method) and peak potentials for the as-prepared systems and after chemical reduction.

	Onset(V)[a]	E_p(V)[a]
GO Foam	-0.300	-0.470
B,N-GO Foam	-0.178	-0.340
S,N-GO Foam	-0.185	-0.356
Red-GO Foam	-0.310	-0.448
Red-B,N-GO foam	-0.158	-0.312
Red-S,N-GP Foam	-0.170	-0.328

[a] The values are calculated for a potential scan rate of 10 mV/s. The potentials are reported vs. the Ag/AgCl/$Cl^-_{(sat.)}$ reference electrode.

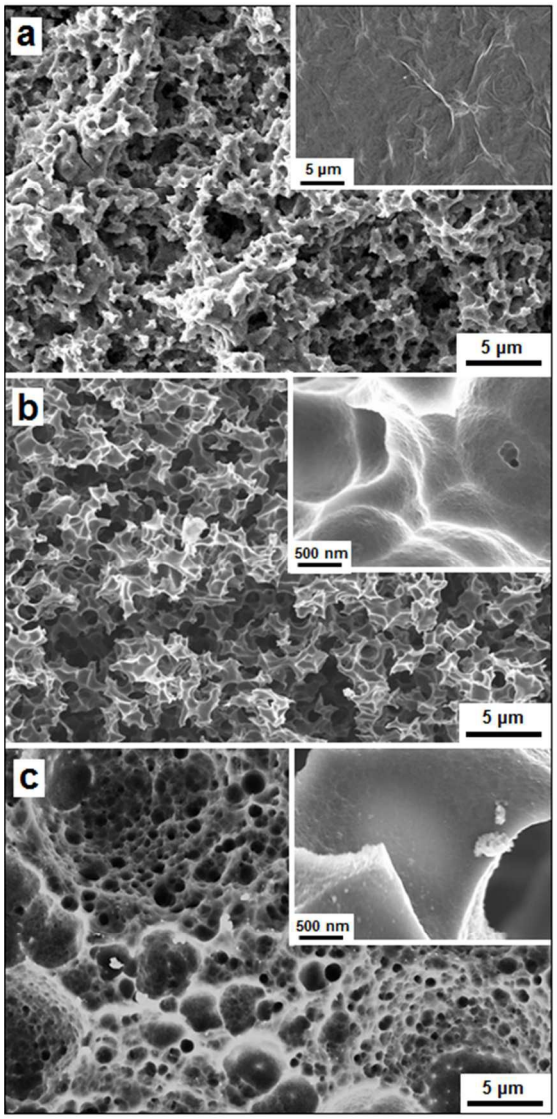

Fig. 8. SEM topographies at different magnifications of pure (a, reported as reference), B,N- (b) and S,N-co-doped GO foams (c). The inset reported in Figure a shows the surface morphology of the as-deposited GO paper on GC before the electrochemical etching.

As reported in Table 4, the doped systems exhibit a positive shift of the onset and of the peak potential with respect to pure GO foam, indicating that the introduction of the heteroatoms promotes the catalytic activity toward the ORR, as also observed for the doped GOQDs. ORR tests have been performed also on the chemically reduced materials to study the catalytic role played by the oxygen functional groups naturally present on the surface of the as-prepared systems, similarly to what has been performed on the corresponding GOQDs. The GO foams have been treated in $NaBH_4$ at r.t. for 12 h. From Figure 9 and Table 4 it is possible to observe that the chemical reduction treatment is beneficial for the enhancement of the electrocatalytic activity of the studied foams, with a net gain of

almost 30 mV in the O_2 reduction peak potentials passing from the as-prepared to the chemically reduced systems. Interestingly, as also observed for the doped-GOQDs, both systems (as-prepared and chemically reduced systems) exhibit a clear decrease of the ORR overpotential as a function of the dopant, according to the sequence pure > S,N > B,N.

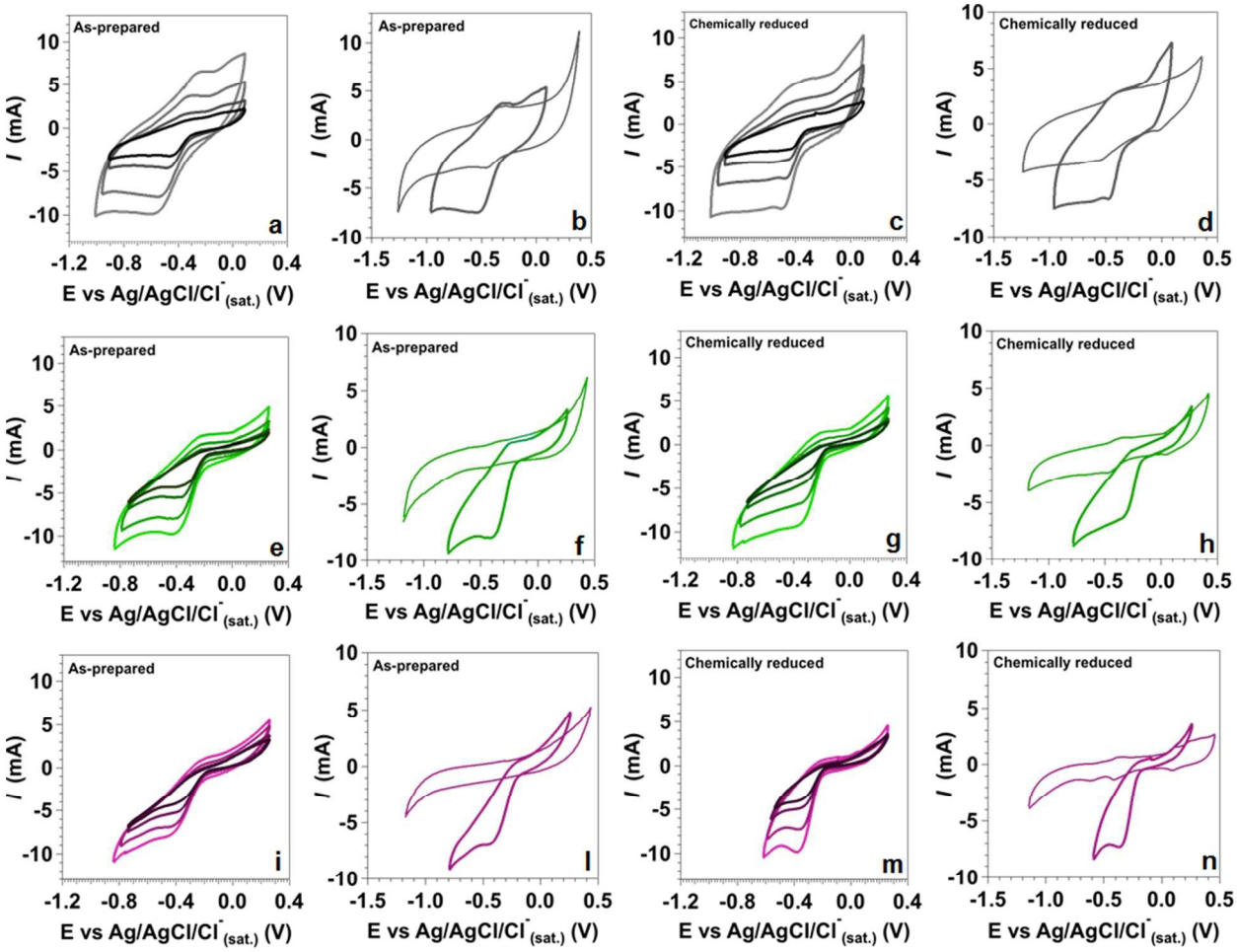

Fig. 9. CV curves at different potential scan rates (10, 20, 50 and 100 mV/s) recorded in O_2-saturated 0.1 M KOH solution for the as-prepared and chemically reduced pure (a, c), B,N- (e, g) and S,N-GO foams (i, m), respectively. Figures b-d, f-h and l-n report the CVs (scan rate 50 mV/s) acquired in Ar- (thin curves) and in O_2-saturated 0.1 M KOH solution (thick curves), for the as-prepared and chemically reduced pure, B,N- and S,N-GO foams, respectively.

D. Water remediation over pure and S,N-GOQDs

For the decomposition of organic pollutants in wastewaters, several procedures are well-known and studied in the literature, such as photo-degradation over photo-active materials, the Fenton process and the decomposition over clay-based catalysts or activated carbons.[79,80,81,82,83] Most of them require the addition of H_2O_2, which serves as the source for highly reactive hydroxyl radicals that are responsible for the molecular degradation of the organic pollutants.[79,82,83] Therefore, the main goal in water remediation is to find an appropriate catalyst that can activate the hydrogen peroxide and produce free radicals during its decomposition.[79-83] The as-prepared doped-GOQDs represent an ideal material for water remediation applications since they can be used at the anode for the selective *in situ* production of H_2O_2 and at the cathode for the decomposition of the latter to OH• radicals, which eventually decompose the organic pollutants. We have used the as-prepared S,N-GOQDs as both cathodic and anodic active material for the electrooxidation/decomposition of phenol in water, using the set-up depicted in Figure 10. To gauge the results, we have used as reference the pure GOQDs,

Figure 11.a reports the polarization curves acquired in PBS solution for both systems. The reported inset shows that the two diffusion peaks are characterized by a large difference in the ORR overpotential, with a net gain of 85 mV in the peak potential of the S,N-GOQDs with respect to the pure GOQDs. Thence, using pure and S,N-GOQDs as both cathode and anode, two different potentiostatic experiments were performed in a solution containing 50 mM of phenol, at -845 mV and at -760 mV, respectively. The decrease of phenol concentration was monitored by colorimetric method as described in the experimental part. Figures 11.b and c report the time evolution of phenol for both experiments.

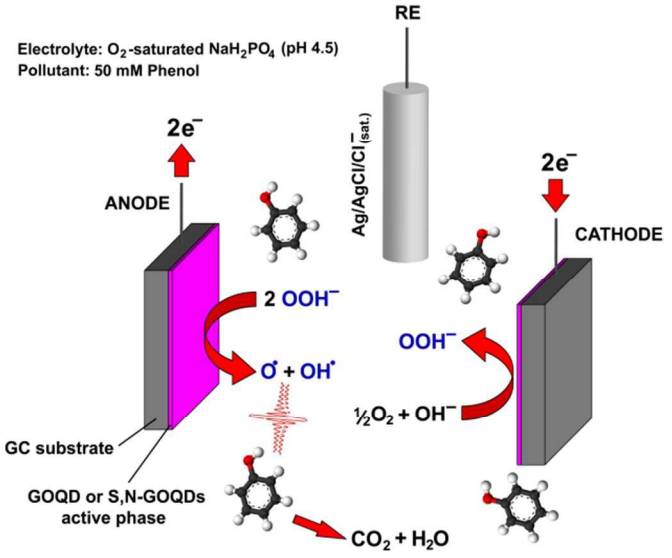

Fig. 10. Pictorial representation of the experimental set-up adopted for for the decomposition of phenol in water mediated by the in-situ production of hydrogen peroxide during the ORR onto as-prepared GOQD systems.

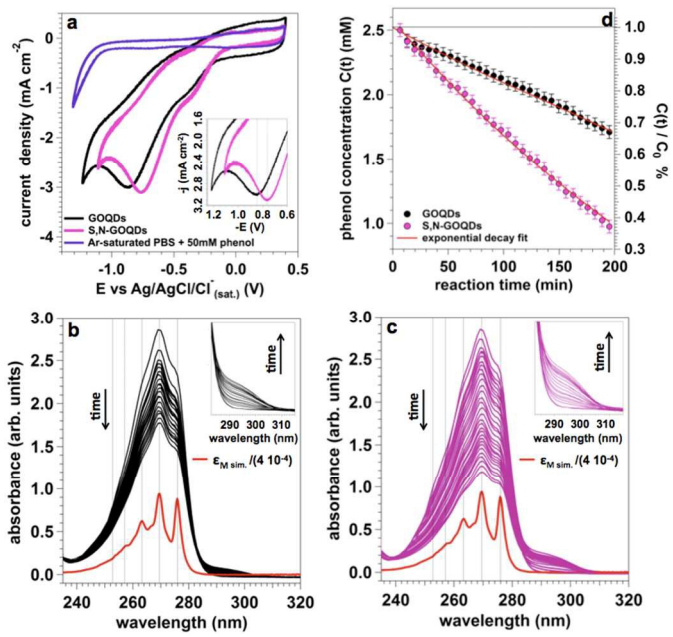

Figure 11. a: CVs in O_2-saturated PBS solution containing phenol, taken at 10 mV/s for pure and S,N-GOQDS (the blank measurement acquired in Ar-purged PBS solution is referred to S,N-GOQDs). The inset reports a zoom of the diffusion peaks for the two systems; b,c: time evolution of the absorbance spectrum for pure and S,N-GOQDs, respectively. The red curve represents the simulation of the ε_M for phenol in PBS solution; the insets report a zoom of the shoulder visible between 290 and 300 nm, probably due to oxidized species; d: evolution of the phenol concentration as a function of the reaction time, for both systems.

The insets show the shoulder between 290 and 300 nm, related to phenol oxidation products. After 200 min, in the S,N-GOQDs system, the absorbance over the phenol spectral window is twice as low as for GOQDs. This observation is confirmed by the trend of the phenol concentration in solution during the reaction, reported for both systems in Figure 11.d.
The phenol degradation kinetics over the S,N-GOQDs is twice as fast as over the GOQDs. In addition, thanks to their high activity toward oxygen reduction, the S,N-GOQDs show a faster kinetic for the decomposition of phenol at a lower overpotential than pure GOQDs.

Experimental Section

Only basic information is reported in the present section. See supporting information (ESI) for more details.

A. Synthesis of pure and doped-GOQDs

The preparation of pure and doped-GOQDs was carried out by the electrochemical etching of a GO Working Electrode (WE), as reported in our previous works.[32,34] The WEs were obtained by deposition of a GO thin film on a polished Glassy Carbon (GC) substrate. The EC syntheses of doped-GOQDs were carried out by adding the molecular precursor chosen as the dopant source to a 0.1 M Phosphate Buffer Solution (PBS) (see Table S1 for the details about the synthesis conditions). The characterization of the prepared materials was carried out by XPS, NEXAFS, UV-Vis absorption spectroscopy, STM and Raman microscopy (see ESI for the corresponding experimental details).

B. ORR catalytic tests on pure and doped-GOQDs

The electrochemical activity measurements toward ORR were carried out by cyclic voltammetry (CV) and rotating disk electrode (RDE) measurements, using an Autolab PGstat 101 potentiostat. A conventional three-electrode configuration consisting of a Pt wire as CE and a saturated Ag/AgCl/Cl^- (standard electrode potential $E^{\Theta}_{Ag/AgCl(sat.)}$= 0.197 V with respect to the standard hydrogen electrode, SHE) as RE was used. All the potentials reported in this work are referred to this RE.
For preparing the catalyst ink, 4 mg of S- or S,N-co-doped-GOQDs were dissolved in 1 mL of bi-distilled water; after the addition of 20 vol % perfluorinated Nafion alcoholic solution (5 wt % , Aldrich), the so-obtained solutions were ultra-sonicated for 30 min. Then, the WEs were prepared by depositing 15 µL of the desired ink onto a polished (see ESI) GC disk mounted in a RDE tip (Autolab RDE-2), which exposed an area of 0.071 cm^2 to the electrolytic medium. Finally, the drop-cast films were dried in air at room temperature (r.t.) for about 12 h. The CV and RDE measurements were performed in 0.1 M KOH, after purging the solutions with Ar before each measurement, whereas the ORR tests were carried out in an O_2 saturated solution.

C. Water remediation: decomposition of phenol

The activity of pure and S,N-co-doped GOQDs toward the decomposition of phenol was estimated by measuring the decomposition rate of this molecule in an aqueous solution. 50 mL of a PBS solution (pH = 4.5), saturated with O_2, were used

as electrolyte in a standard three-electrode EC cell, using a saturated Ag/AgCl/Cl^- as RE. The WE and CE were prepared by drop-casting 250 µL of pure or S,N-co-doped GOQDs solution (3.0 mg mL-1 + 5% vol. of perfluorinated Nafion alcoholic solution, Aldrich) onto a polished GC substrate (3.0 cm^2). The cell was enveloped with aluminum foil to prevent light-induced decomposition of phenol. The electrolyte was kept at 25 °C during the synthesis by a thermostatic water bath. The stirring of the electrolytic medium during the reaction was maintained by a magnetic mixer. The electrochemical measurements were carried out by a EG&G PARC 173 potentiostat/galvanostat. The phenol degradation experiments were performed by introducing 235 mg of phenol (>99.0 %, Aldrich) in the described system, which correspond to a concentration of 50 mM. The degradation tests were performed under potentiostatic conditions for about 3.5 h. Phenol degradation was measured by withdrawing small aliquots of the aqueous solution (50µL, to avoid possible perturbations of the reaction environment) at regular time intervals during the reaction.

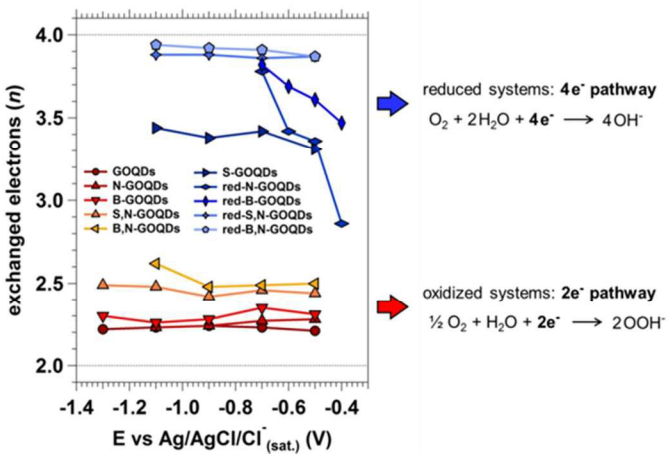

Fig. 12. Trend of the number of exchanged electrons as a function of the cathodic potential, for the as-prepared and the chemically-reduced GOQDs.

Conclusion

In this work, we have reported a simple electrochemical route for the preparation doped graphene materials both in the form of nanometric quantum dots and of there-dimensional materials characterized by a hierarchical porous morphology. This method is quite general, allows the introduction of several dopants such as B, N, S and of any combination of them, and can be conveniently performed at r.t. in aqueous environment without the use of toxic or hazardous chemicals.

The introduction of dopants can boost the ORR; especially in the case of co-doped materials that show a very low overpotential. Moreover, the chemical activity of doped-GOQD can be selectively driven toward a four electron reduction path (i.e. direct reduction of O_2 to water) by simple chemical reduction with $NaBH_4$. This treatment has the twofold effect of increasing the catalytic activity and eliminating the oxygen species that are responsible for the competitive bi-electronic reaction. Figure 12 summarizes the experimental observations for the various as-prepared and chemically-reduced systems studied in this work. Furthermore, we have shown that GOQDs in oxidized form, represent suitable catalysts for phenol degradation. Their high selectivity for the two electron ORR pathway can be fruitfully employed for the *in-situ* generation of hydrogen peroxide. Moreover, the use of the set-up shown in Figure 11 affords the electrochemical activation of H_2O_2 into free radicals that can efficiently promote decomposition reactions in pollutant-containing aqueous solutions (such as laboratory or industrial waste waters). Finally, the use of S,N-GOQDs provides lower overpotential values and higher degradation efficiencies than the use of pure GOQDs.

Acknowledgements

MF acknowledges Fondazione Cariparo for financial support. LC and MS acknowledge the PRIN Project "DESCARTES" (Project No. 2010BNZ3F2). We acknowledge also financial support from the Fuel Cell and Hydrogen Initiative - Joint Undertaking (FCH-JU) within the CathCat project under contract No. 303492, by the Italian MIUR through the national grant Futuro in Ricerca 2012 RBFR128BEC "Beyond graphene: tailored C-layers for novel catalytic materials and green chemistry" and by the University of Padova funded project: CPDA128318/12 "Study of the catalytic activity of complex graphene nanoarchitectures from ideal to real conditions".

Notes and references

[a] Department of Chemical Sciences Via F. Marzolo 1 35131 Padova E-mail: stefano.agnoli@unipd.it

[b] current address: Advanced Light Source (ALS) Joint Center for Artificial Photosynthesis (JCAP) Lawrence Berkeley National Laboratory 1 Cyclotron Rd., M/S 6R2100 Berkeley, CA 94720

† Electronic Supplementary Information (ESI) available: experimental details, Tafel plots, Koutecky-Levich analysis, durability and tolerance tests, XPS spectra of foams. See DOI: 10.1039/b000000x/

References

1 D. R. Dreyer, S. Park, C. W. Bielawski and R. S. Ruoff, *Chem. Soc. Rev.*, 2010, **39**, 228-240.

2 O. C. Compton and S. T. Nguyen, *Small*, 2010, **6**, 711-723

3 Y. Zhu, S. Murali, W. Cai, X. Li, J. W. Suk, J. R. Potts and R. S. Ruoff, *Adv. Mater.*, 2010, **22**, 3906-3924.

4 H. Bai, C. Li and G. Shi, *Adv. Mater.*, 2011, **23**, 1089-1115.

5 S. Agnoli and G. Granozzi, *Surf. Sci.*, 2013, **609**, 1-5.
6 C. H. Choi, M. W. Chung, H. C. Kwon, S. H. Park, and S. I. Woo, *J. Mater. Chem. A,* 2013, **1**, 3694-3699.
7 D. Haag, H. H. Kung *Topics in Catalysis*, 2014, **57**, 762-773
8 P. P. Upare, J.-W. Yoon, M. Y. Kim, H.-Y. Kang, D. W. Hwang, Y. K. Hwang, H. H. Kung, J.-S. Chang *Green Chem.,* 2013,**15**, 2935-2943
9 D. W. Wang and D. Su, *Energy Environ. Sci.*, 2014, **7**, 576-591
10 G. Wu and P. Zelenay, *Acc. Chem. Res.*, 2013, **46**, 1878-1889.
11 S. Wang, L. Zhang, Z. Xia, A. Roy, D. W. Chang, J.-B. Baek and L. Dai, *Angew. Chem. Int. Ed.*, 2012, **51**, 4209-4212
12 Y. Zheng, Y. Jiao, L. Ge, M. Jaroniec and S. Z. Qiao, *Angew. Chem. Int. Ed.*, 2013, **52**, 1-7.
13 J. Liang, Y. Jiao, M. Jaroniec and S. Z. Qiao, *Angew. Chem. Int. Ed.*, 2012, **51**, 11496-11500.
14 S. Yang, L. Zhi, K. Tang, X. Feng, J. Maier and K. Müllen, *Adv. Funct. Mater.*, 2012, **22**, 3634-3640.
15 Y. Chen, J. Li, T. Mei, X. Hu, D. Liu, J. Wang, M. Hao, J. Li, J. Wang, X. Wang *J. Mater. Chem. A*, 2014, **2**, 20714-20722
16 M. Cattelan, S. Agnoli, M. Favaro, D. Garoli, F. Romanato, M. Meneghetti, A. Barinov, P. Dudin, G. Granozzi, *Chem. Mater.* 2013, **25**, 1490-1495.
17 Z. Zuo, Z. Jiang, A. Manthiram, *J. Mater. Chem. A*, 2013,**1**, 13476-13483.
18 Z. Yang, Z. Yao, G. Li, G. Fang, H. Nie, Z. Liu, X. Zhou, X. Chen and S. Huang, *ACS Nano*, 2012, **6**, 205-211.
19 H. Wang, T. Maiyalagan and X. Wang, *ACS Catal.*, 2012, **2**, 781-794.
20 L. Qu, Y. Liu, J.-B. Baek and L. Dai, *ACS Nano*, 2010, **4**, 1321-1326.
21 Y. Xue, D. Yu, L. Dai, R. Wang, D. Li, A. Roy, F. Lu, H. Chen, Y. Liu and J. Qu, *Phys. Chem. Chem. Phys.*, 2013, *15*, 12220-12226.
22 D. Geng, N. Ding, T. S. A. Hor, Z. Liu, X. Sun, Y. Zong *J. Mater. Chem. A*, 2015,**3**, 1795-1810
23 S. N. Baker and G. A. Baker, *Angew. Chem. Int. Ed.*, 2010, **49**, 6726-6744.
24 L. Li, G. Wu, G. Yang, J. Peng, J. Zhao, J.-J. Zhu, *Nanoscale*, 2013, **5**, 4015-4038.
25 D. Qu, M. Zheng, P. Du, Y. Zhou, L. Zhang, D. Li, H. Tan, Z. Zhao, Z. Xie and Z. Sun, *Nanoscale*, 2013, **5**, 12272-12277.
26 X. Yan, X. Cui and L.S. Li, *J. Am. Chem. Soc.*, 2010, **132**, 5944-5945.
27 G. Eda, Y.-Y. Lin, C. Mattevi, H. Yamaguchi, H.-A. Chen, I.-S. Chen,C.-W. Chen and M. Chhowalla, *Adv. Mater.*, 2010, **22**, 505-509.
28 J. Tobik, A. Dal Corso, S. Scandolo and E. Tosatti, *Surf. Sci.,* 2004, **566-568**, 644-649.
29 H. Sun, L. Wu, W. Wei, X. Qu and J.-J. Zhu, *Materials Today*, 2013, **16**, 433-442.
30 Z. Zhang, J. Zhang, N. Chen and L. Qu, *Energy Environ. Sci.,* 2012, **5**, 8869-8890.
31 G. S. Kumar, R. Roi, D. Sen, U. K. Ghorai, R. Thapa, N. Mazumder, S. Saha and K. K. Chattopadhyay, *Nanoscale*, 2014, **6**, 3384-3391.
32 M. Favaro, S. Agnoli, M. Cattelan, A. Moretto, C. Durante, S. Leonardi, J. Kunze-Liebhäuser, O. Schneider, A. Gennaro and G. Granozzi, *Carbon*, 2014, **77**, 405-415.
33 Y. Li, Y. Hu, Y. Zhao, G. Shi, L. Deng, Y. Hou and L. Qu, *Adv. Mater.*, 2011, **23**, 776-780.
34 M. Favaro, L. Ferrighi, G. Fazio, L. Colazzo, C. Di Valentin, C. Durante, F. Sedona, A. Gennaro, S. Agnoli, G. Granozzi, *ACS Catalysis*, 2015, **5**, 129-144.
35 I.-Y. Jeon, S. Zhang, L. Zhang, H.-J. Choi, J.-M. Seo, Z. Xia, L. Dai J.-B. Baek, *Adv. Mater.*, 2013, **25**, 6138-6145.
36 C. H. Choi, S. H. Park and S. I. Woo, *ACS Nano*, 2012, **6**, 7084-7091.
37 H. Fei, R. Ye, G. Ye, Y. Gong, Z. Peng, X. Fan, E. L. G. Samuel, P. M. Ajayan and J. M. Tour, *ACS Nano*, 2014, **8**, 10837-10843.
38 Z. Liu, H. Nie, Z. Yang, J. Zhang, Z. Jin, Y. Lu, Z. Xiao and S. Huang, *Nanoscale*, 2013, **5**, 3283-3288.
39 S.-A. Wohlgemuth, R. J. White, M.-G. Willinger, M. M. Titirici, M. Antonietti, *Green Chem.*, 2012, **14**, 1515-1523.
40 S.-A. Wohlgemuth, F. Vilela, M. M. Titirici and M. Antonietti, *Green Chem*., 2012, **14**, 741-749.
41 V. Lee, L. Whittaker, C. Jaye, K. M. Baroudi, D. A. Fischer and S. Banerjee, *Chem. Mater.*, 2009, **21**, 3905-3916.
42 S. Saxena, T. A. Tyson and E. Negusse, *J. Phys. Chem. Lett.*, 2010, **1**, 3433-3437.
43 A. Hunt, D. A. Dikin, E. Z. Zurmaev, T. D. Boyko, P. Bazylewski, G. S. Chang and A. Moewes, *Adv. Funct. Mater.*, 2012, **22**, 3950-3957.
44 D. Brete, D. Przyrembel, C. Eickhoff, R.Carley, W. Freyer, K. Reuter, C. Gahl and M. Weinelt, *J. Phys.: Condens. Matter*, 2012, **24**, 394015.
45 L.-S. Zhang, X.-Q. Liang, W.-G. Song and Z.-Y- Wu, *Phys. Chem. Chem. Phys*., 2010, **12**, 12055-12059.
46 M.S. Dresselhaus, A. Jorio and R. Saito, *Annu. Rev. Condens. Matter Phys.*, 2010, **1**, 89-108.
47 A.C. Ferrari and D. M. Basko, *Nat. Nanotech.*, 2013, **8**, 235-246.
48 S. Kim, D. H. Shin, C. O. Kim, S. S. Kang, S. S. Joo, S.-H. Choi, S. W. Hwang and C. Sone, *Appl. Phys. Lett.* 2013, **102**, 053108.
49 Y. A. Kim, K. Fujisawa, H. Muramatsu, T. Hayashi, M. Endo, T. Fujimori, K. Kaneko, M. Terrones, J. Behrends, A. Eckmann, C. Casiraghi, K. S. Novoselov, R. Saito, M. S. Dresselhaus, *ACS Nano*, 2012, **6**, 6293 -6300.
50 A. C. Ferrari, *Solid State Commun*., 2007, **143**, 47-57.
51 K. Ritter, J. Lyding *Nat. Mater.* 2009, **8**, 235 - 242
52 Y. Kobayashi, K. Fukui, T. Enoki, K. Kusakabe, Y. Kaburagi *Phys. Rev. B* 2005, **71**, 193406
53 F. Liu, M.-H. Jang, H. D. Ha, J.-H- Kim, Y.-H. Cho and T. S. Seo, *Adv. Mater.,* 2013, **25**, 3657-3662.
54 Z. Gan, S. Xiong, X. Wu, T. Xu, X. Zhu, X. Gan, J. Guo, J. Shen, L. Sun, P. K. Chu *Adv. Optical. Mater.* 2013, **1**, 926-932
55 S. Zhu, L. Wang, B. Li, Y. Song, X. Zhao, G. Zhang, S. Zhang, S. Lu, J. Zhang, H. Wang, H. Sun, B. Yang, *Carbon* 2014, **77**, 462-472
56 W. Kwon, S. Do, J. Lee, S. Hwang, J. K. Kim and S.-W. Rhee, *Chem. Mater.,* 2013, **25**, 1893-1899.

57 Y. Li, Y. Zhao, H. Cheng, Y. Hu, G. Shi, L. Dai and L. Qu, *J. Am. Chem.Soc.*, 2012, **134**, 15-18.
58 K. P. Gong, F. Du, Z. H. Xia, M. Durstock and L. M. Dai, *Science,* 2009, **323**, 760-764.
59 S. Y. Wang, D. S. Yu and L. M. Dai, *J. Am. Chem. Soc.*, 2011, **133**, 5182-5185.
60 L. Wang, S.-J. Zhu, H.-Y. Wang, S.-N. Qu, Y.-L. Zhang, J.-H. Zhang, Q.-D. Chen, H.-L. Xu, W. Han, B. Yang, H.-B. Sun, *ACS Nano* 2014 **8** 2541–2547.
61 G. S. Kumar, R. Roy, D. Sen, U. K. Ghorai, R. Thapa, N. Mazumder, S. Saha, K.K. Chattopadhyay, *Nanoscale* 2014, **6**, 3384-3391.
62 B.-X. Zhang, H. Gao and X.-L. Li, *New J. Chem.,* 2014, **38**, 4615-4621.
63 Y. Dong, H. Pang, H. B. Yang, C. Guo, J. Shao, Y. Chi, C. M. Li and T. Yu, *Angew. Chem. Int. Ed.,* 2013, **52**, 7800-7804.
64 D. Qu, M. Zheng, P. Du, Y. Zhou, L. Zhang, D. Li, H. Tan and Z. Zhao, *Nanoscale*, 2013, **5**, 12272-12277.
65 W. M. Haynes, *Handbook of Chemistry and Physics*, CRC Press, Boca Raton, FL, 2005
66 I.-Y. Jeon, S. Zhang, L. Zhang, H.-J. Choi, J.-M. Seo, Z. Xia, L. Dai, J.-B. Baek, *Adv. Mater.* 2013, **25**, 6138–6145
67 L. Zhang, J. Niu, M.Li, Z.Xia *J. Phys. Chem. C*, 2014, **118**, 3545−3553.
68 Y. Jiao, Y. Zheng, M. Jaroniec, S. Z. Qiao *J. Am. Chem. Soc.* 2014, *136*, 4394−4403.
69 W. Yuan, Y. Zhou, Y. Li, C. Li, H. Peng, J. Zhang, Z. Liu, L. Dai, G. Shi, *Sci. Rep.*, 2013, **3**, 2248.
70 J. Bart, L. R. Faulkner, *Electrochemical Methods*, Wiley, 2001.
71 I. Morcos, E. Yeager, *Electrochim. Acta,* 1970, **15**, 953–75
72 J.-H. Zhong, J. Zhang, X. Jin, J.-Y. Liu, Q. Li, M.-H. Li, W. Cai, D.-Y. Wu, D. Zhan, B. Ren, *J. Am. Chem. Soc.* 2014, *136*, 16609.
73 J. Y. Cheon, J. H. Kim, J. H. Kim, K. C. Goddeti, J. Y. Park, S. H. Joo *J. Am. Chem. Soc.* 2014, **136**, 8875−8878
74 T. Xing, Y. Zheng, L. H. Li, B. C. C. Cowie, D. Gunzelmann, S. Z. Qiao, S. Huang and Y. Chen, *ACS Nano*, 2014, **8**, 6856-6862.
75 W. Y. Wong, W. R. W. Daud, A. B. Mohamad, A. A. H. Kadhum, K. S. Loh and E. H. Majlan, *Intern. J. Hydrogen Energ.*, 2013, **38**, 9370-9386.
76 T. Sun, S. Fabris, Nano Lett., 2012, **12**, 17-21.
77 Z. Li, W. Zhang, Y. Juo, J. Yang and J. G. Hou, *J. Am. Chem. Soc.*, 2009, **131**, 6320-6321.
78 T. Palaniselvam, M. O. Valappil, R. Illathvalappil S. Kurungot *Energy Environ. Sci.*, 2014, **7**, 1059–1067.
79 K. Kabra, R. Chaudhary and R. L. Sawhney, *Ind. Eng. Chem. Res.*, 2004, **43**, 7683-7696
80 Y. Zheng, J. Liu, M. Jaroniek and S. Z. Qiao, *Energy Environ. Sci.*, 2012, **5**, 6717-6731
81 G. Liu, P. Niu, C. Sun, S. C. Smith, Z. Chen, G. Q. Lu and H.-M. Cheng, *J. Am. Chem. Soc.*, 2010, **132**, 11642-11648.
82 F. Lücking, H. Köser, M. Jank and A. Ritter, *Wat. Res.* 1998, **32**, 2607-2614.
83 J. Guo and M. Al Dahhan, *Ind. Eng. Chem. Res.,* 2003, **42**, 2450-2460.